Journal of the Korean Nuclear Society
Volume 29, Number 6, pp451~458, December 1997

Signal Shapes from a Closed-ended Coaxial HPGe Detector

H.D. Choi
Seoul National University
San 56-1, Shinlim-dong, Kwanak-gu, Seoul 151-742, Korea
(Received February 24, 1997)

Abstract

Signal shapes from a closed-ended coaxial HPGe detector are investigated by numerical methods. The detector used in this study has a volume of 72 cm^3 with relative efficiency of 15%. The electric field and potential distributions in the detector are determined by solving the Poisson equation at the depletion and operating bias. Hence the time dependent signal shapes induced on the electrode are obtained from the energy balance consideration and by solving the equation of motion for the charge carriers. For various initial positions of a charge carrier pair, the collection times of induced charge vary in the range of 70 - 404 nsec.

1. Introduction

The closed-ended coaxial HPGe detector of a large volume has been widely applied for low-level γ-ray measurement and spectroscopy [1]. The present study is concerned about the timing properties of a closed-ended coaxial HPGe detector. The obtained information will be useful in the field of spectroscopic application utilizing the coincidence-anticoincidence techniques for the experiments involving multiple-γ detectors or β-γ detectors.

For the case of true coaxial HPGe detectors, the potential distribution in the detector and signal shape of induced charges are known in an analytic form [2-4]. The problem for a closed-ended detector, however, is far complicated due to its geometry. Moreover, the presence of space charge at the impurity sites further complicates the calculation. Though the pulse shapes can be obtained by measurement, the position of interaction can not be known but may be dispersed through the detector for γ-rays of energy larger than several hundred keV. Therefore only theoretical and numerical approach to the problem is feasible herein for the closed-ended type of HPGe detectors [5,6]. The detector used in this study is a p-type crystal of 72 cm^3 volume and the relative efficiency is 15%. It is being used for γ-spectroscopy in the departmental laboratory.

To obtain the potential and electric field distributions for depletion and operating conditions, the Poisson equation is solved by iterative method on the discretized mesh points in two dimensional cross section of the detector. By integrating the equation of motion for charge carriers, the time dependent positions of electrons and holes are determined. Hence signal shapes induced on the electrode are calculated on the basis of energy balance principle. Since the trajectory and motion of charge carriers are followed from the initial position, the collection of charge signal varies depending on the position of ionizing interaction. For several representative positions of initial

charge carriers, signal shapes are shown explicitly. From the calculated signal shapes, the charge collection time and signal rise time are determined.

2. Theoretical Calculation

2.1. The Electric Field and Potential Distribution

The closed-ended detector under study has a p-type crystal of 36.5 mm length, 50.5 mm diameter with a core hole of 7.5 mm diameter and 22 mm depth. The cross section of the detector crystal is shown in Fig. 1. The detector was fabricated by Canberra Industries, Inc. A detailed specification is listed in Table 1 as provided by the manufacturer. Information about the so called bulletization is not available and hence the geometry of the detector is assumed as a circular cylindrical shape with a core hole of sharp edge.

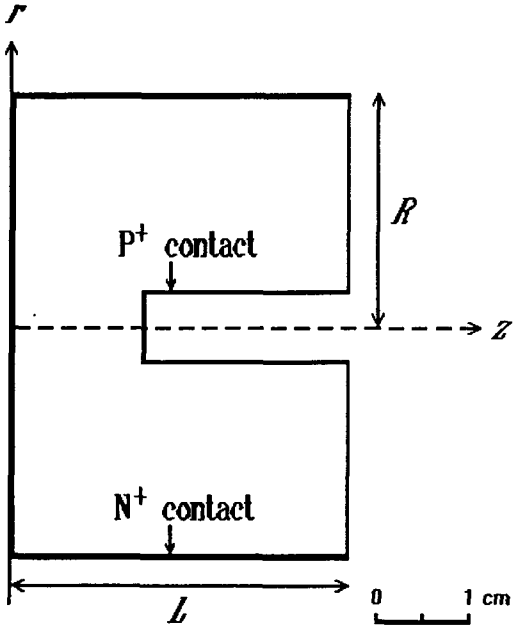

Fig. 1. A Cross Sectional View of the Detector Crystal (L=36.5 mm, R = 25.25 mm).

Table 1. Specification of the Closed-ended HPGe Detector

Relative efficiency	15%
Resolution (FWHM)	1.73 keV for 1.33 MeV γ-ray
	0.84 keV for 122 keV γ-ray
Geometry	closed-ended coaxial
Crystal diameter (2R)	50.5 mm
Crystal length (L)	36.5 mm
Core diameter	7.5 mm
Core height	22 mm
Outer surface contact	Li-diffused N^+ contact
	(thickness : 0.5 mm)
Well surface contact	B-implanted P^+ contact
	(thickness : 0.3 μm)
Detector depletion voltage	+2000 V
Detector bias voltage	+3000 V
Detector capacitance	~14 pF

The potential inside a typical semiconductor detector is described by the Poisson equation

$$\nabla^2 u = -\frac{e}{\varepsilon}\left(p - n + N_d^+ - N_a^-\right) \quad (1)$$

where u is the potential, p and n are the hole and the electron concentrations, respectively, N_d^+ and N_a^- are the ionized donor and acceptor impurity concentrations, respectively, e is the magnitude of electronic charge and ε is the permittivity of germanium which is 16 times that of vacuum value. When the mobile charges inside the detector are fully depleted, the charge density is solely determined by the impurity level. If the cylindrical coordinates (r, z, ϕ) are introduced with z-axis as the rotational symmetry axis and with the origin at the center of the frontal detector face (Fig. 1), equation (1) is given by

$$\frac{1}{r}\frac{\partial}{\partial r}\left(r\frac{\partial u}{\partial r}\right) + \frac{\partial^2 u}{\partial z^2} = \frac{e}{\varepsilon}N \quad (2)$$

after cancelling the symmetric ϕ-dependent term. Here $N = N_a^- - N_d^+ \cong N_a^-$ is the impurity level in the high purity p-type Ge single crystal. Boundary conditions are imposed on both electrodes. The

lithium-diffused outer surface is held at constant positive potential of the applied voltage, while the boron implanted well surface is grounded. The Neumann condition is imposed on the open part of coaxial region such that the surface normal component of the electric field vanishes.

Several methods are available to solve the equation (2) by numerical procedures [7]. One of the widely useful methods is the reduction of the differential equation into a large number of algebraic equations based on the finite difference method. The present study follows a CERN routine [8], with proper modifications, which solves elliptic partial differential equation defined on a bidimensional domain with a mixed boundary condition, i.e. with both Dirichlet and Neumann conditions. The routine is written in FORTRAN and is implemented on an IBM PC. The program can determine the electric field and potentials at a maximum number of 2900 mesh points. The iterative solution is found to approach the true solution by means of a successive overrelaxation method where the accelerating factor of convergence is taken from Carré 's prescription [9]. Since there is a symmetry, only half region of the (r, z) cross sectional domain of the detector is divided by a mesh size of Δr = 0.75 mm, Δz = 0.5 mm. The thicknesses of inner and outer contact layer are neglected by comparison with the size of discretization in the computation. Stopping condition of the iteration process is that the maximum of estimated relative errors of the numerical potentials at mesh points should be below 1%. Typical number of iterations required before stopping is in the range of 70 - 110. The accuracy of the written algorithm is checked by comparing the numerical solution with the exact analytic solution for the problem of true coaxial geometry [2]. The consistency of both results is of the order of accuracy criterion for stopping iterations (0.5 - 1.0%).

The impurity level of the detector in this study is not known exactly. A typical HPGe has the impurity concentration less than 10^{10} cm^{-3} [5,10,11]. Hence the level is determined on a trial method. By assuming that the depletion voltage of 2000 V is an accurate value, the impurity concentration is determined from repeated trial calculations such that all of the calculated potential values in the detector have the same positive sign. For a uniform impurity level, the concentration turned out to be $1.3 \times 10^{10} cm^{-3}$.

After the impurity level is determined, the electric field and potential distributions are obtained in a straightforward way by changing only the boundary potential values at the outer contact electrode for depletion and operating condition, respectively. Fig. 2 shows the distributions of potential and electric field strength when the depletion bias is applied to the detector. In Fig. 3, those distributions as in Fig. 2 are shown for the operating condition. By considering the symmetry of the detector, only a half domain is shown in the figures.

2.2. The Pulse Shapes

For planar or coaxial cylindrical detector geometry, the time dependent variation of induced signal is permitted to be described in a closed form from considering the energy balance. A similar procedure is applied to closed-ended detector in numerical approach. If the "short circuit" condition is met, the energy acquired by charge carriers in the course of charge collection is balanced by the dissipation of stored energy in the detector capacitance. The infinitesimal induced charge, therefore, is given by [6]

$$V_A dQ = dW \tag{3}$$

where V_A is the applied bias, dQ is the induced charge and dW is the work done on the charge

carriers by the applied voltage. If the potential distribution by the applied bias only is denoted $U_0(r,z)$, U_0 is obtained from the solution of Laplace equation using the program described previously. Hence the work done on the charge carriers is given by the sum of two parts as

$$dW = dW_e + dW_h = q(dU_0)_e - q(dU_0)_h \quad (4)$$

where the subscripts e and h denote the parts on electron and on hole, respectively, q is the magnitude of electronic charge. From equations (3) and (4), it gives

$$\frac{Q(t)}{q} = \frac{1}{q}\int_0^t dQ = \frac{1}{V_A}\left[\, U_0(\vec{r_e}(t)) - U_0(\vec{r_h}(t))\,\right] \quad (5)$$

where $\vec{r_e}(t)$ and $\vec{r_h}(t)$ are the positions of electron and hole, respectively, at time t. The positions of charge carriers are determined by integrating the equation of motion,

$$\frac{d\vec{r_e}}{dt} = -\mu_e(E)\,\vec{E}(\vec{r_e}) \quad (6)$$

$$\frac{d\vec{r_h}}{dt} = \mu_h(E)\,\vec{E}(\vec{r_h}) \quad (7)$$

where μ_e, μ_h is the mobility of the electron and of the hole, respectively, and $\vec{E}$ is the electric field due to both the applied bias and the space charges at impurity centers. The integration of equation (6) and (7) has been approximated by the sum of successive values in the right hand side at a small

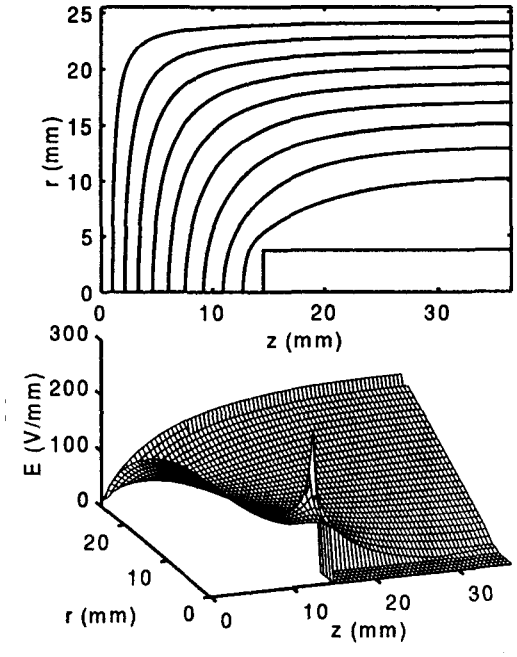

Fig. 2. The Potential Distribution (top) and the Electric Field Strength (bottom) for Depletion Condition of the Detector. The Equipotential Lines are Drawn at 200 V Interval. The Potential at the N^+ Contact is +2000 V and the P^+ Contact is Grounded.

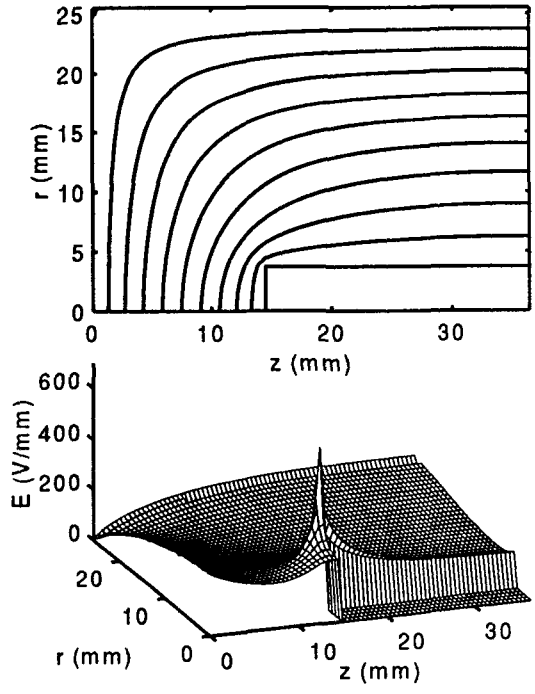

Fig. 3. The Potential Distribution (top) and the Electric Field Strength (bottom) for Operation Condition of the Detector. The Equipotential Lines are Drawn at 300 V Interval. The Applied Voltage is +3000 V.

interval of t. Here the initial position of charge carriers is $\vec{r_e}(0) = \vec{r_h}(0) = \vec{r_i} = (r_i, z_i)$ by assuming that only a pair of electron-hole is generated. The electric field at each position of electron and hole is obtained by cubic interpolation of those at mesh points. The mobility is dependent on the strength of the electric field and is used in the form of

$$\mu(E) = \frac{\mu_0}{1 + (E/E_0)} \tag{8}$$

where μ_0, E_0 are the fitting parameters for the experimental data at 80 K [12]. For electron, $\mu_0 = 3.63 \times 10^6\ mm^2/Vsec$, $E_0 = 27.5\ V/mm$ and for hole, $\mu_0 = 2.49 \times 10^6\ mm^2/Vsec$, $E_0 = 38.5\ V/mm$ are used [3]. The time interval of 1 nsec is enough for accurate and smooth results of integration. Fig. 4 shows some trajectories of charge carriers. The figure also represents the electric field configuration in the detector. Since the positive bias is applied to the n^+ contact electrode, the electron moves towards the outer contact electrode while the hole towards the inner one. By

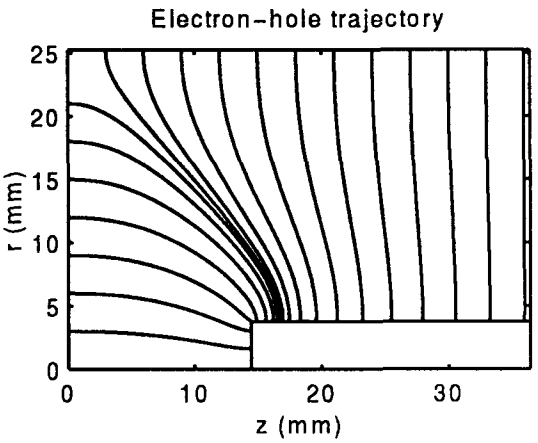

Fig. 4. A Schematic Trajectory of Electron or Hole. The Electron Moves Towards the Outer Electrode While the Hole Towards the Inner One.

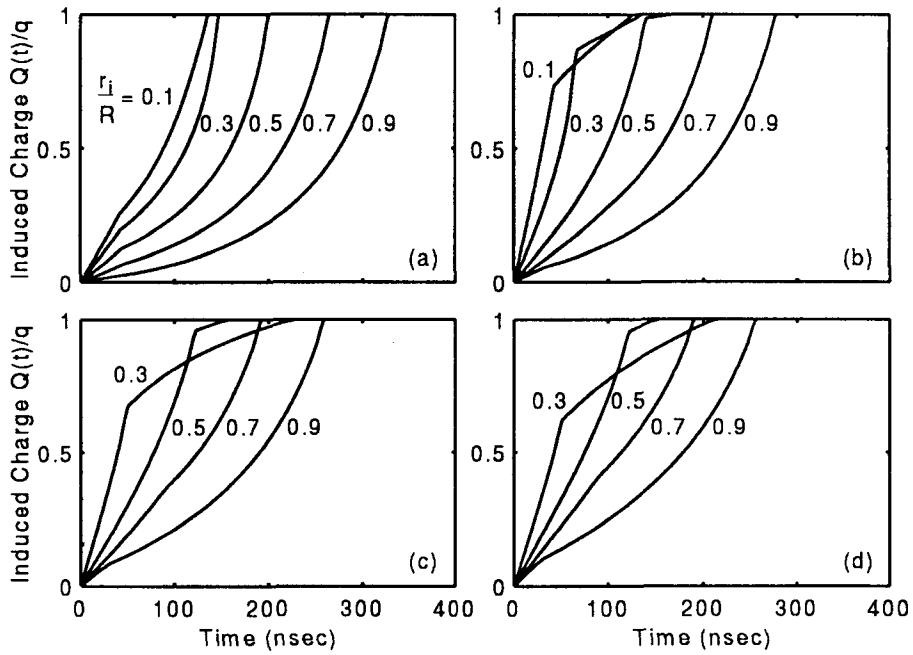

Fig. 5. The Induced Signal Shapes for Various Initial Positions of a Charge Carrier Pair. The Initial Axial Positions (z_i/L) are 0.1 (a), 0.3 (b), 0.5 (c) and 0.7 (d), Respectively. The Initial Radial Positions (r_i/R) are Indicated by the Lines.

using the positions of charge carriers as a function of time, the induced signal is obtained according to equation (5). In Fig. 5, the signal shapes are shown for various initial positions of the charge carriers.

3. Results and Discussion

The electric fields at depletion voltage (Fig. 2) distribute in the range of 0 - 205 *V/mm*. The presence of zero field strength indicates that the detector is fully depleted at the applied bias (2000 *V*) condition and at the impurity concentration of 1.3×10^{10} cm^{-3}. The field distribution in the coaxial part of the detector has a similar feature as that in the true coaxial detector [2]. Due to the geometry, the corner edge region in the frontal part has smaller field strength, while the sharp edge of the core hole has the maximum field strength. The potential distribution is shown in terms of equipotential lines in 200 V spacing. Fig. 3 shows that the electric field strength is enhanced to 20 - 635 *V/mm* at the operation bias (3000 *V*). The distribution of field strength becomes increased and more flattened than that of the depletion condition. Especially the region in the coaxial part around the core hole has enhanced fields. The field enhancement is, however, trivial at the corner edge of the front part. The location of the maximum field strength remains the same as in the case of depletion. The potential distribution is shown by the equipotential lines of 300 *V* spacing.

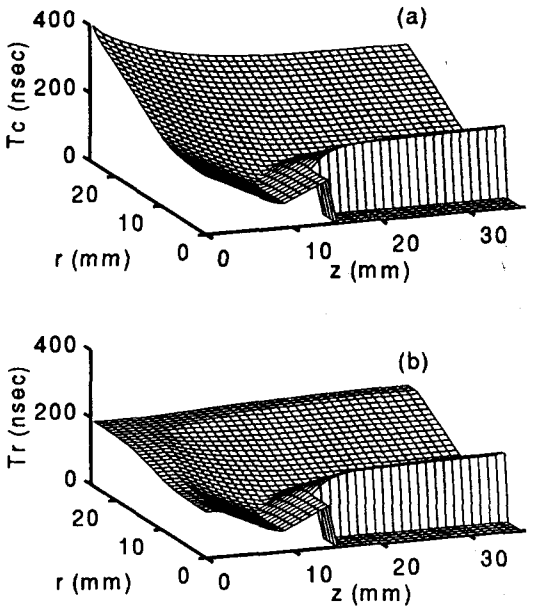

Fig. 6. (a) The Charge Collection Time T_c (0-90%) and (b) the Signal Risetime T_r (10 - 90%) are Shown as a Function of the Initial Position of the Charge Carrier.

Fig. 4 shows typical trajectories of electron and hole at an arbitrary interval. They represent the electric field lines of operational potential distribution which is shown in Fig. 3. The simulated time response of the detector is shown in Fig. 5 for various different interaction points. The kink in the pulse shape corresponds to the collection of either electron or hole, at an electrode. By defining the "charge collection time" as the time taken for 0 - 90% charge collection, it is in the range of 70 - 404 nsec. A remarkably slow pulse gives rise to in the outer region of the closed-ended part, e.g. that of r/R = 0.9, z/L = 0.1 in Fig. 5(a). In this case, the reason is due to the low field strength and the longer trajectory. This is also evident from Fig. 6(a) where the charge collection time is shown as a function of the initial position of charge carriers. Another useful information about timing property is obtained by studying the risetime of 10 - 90% signal rise. Fig. 6(b) shows the distribution of signal risetime. The signal risetime varies in the range of 59 - 220 nsec. An interesting feature in the risetime distribution is that it is relatively flat in the outer surface region of the detector where the charge collection times are large and vary considerably. Due to the difference in mobilities of electron and hole, faster rising pulses occur for the

interactions somewhere between the two electrodes. This region is shown as a valley in Fig. 6.

If the experimental situation is such that the timing information is obtained at the first 10% charge fraction, the slow rising pulses are attributed to the delay and time walk. The timing of 10% charge fraction varies in the range of 3 - 211 nsec for the detector in this study. Reduction in the charge fraction of the timing will be augmented by the contribution of the noise hence a compromise will be purely experimental work. The slow risetime reject technique will also be helpful to improve time walk at the expense of detection efficiency [3].

4. Conclusions

The information on the electric field, potential distribution and the timing properties of detector is required for a detailed analysis of detector performance in coincidence experiment. The field and potential distributions are also necessary to know about the charge collection efficiency in closed-ended HPGe detector [13]. The present study has shown that a theoretical modelling can be realistically solved to get the informations about the electric field, potential distribution, the induced pulse shape and timing properties in closed-ended coaxial HPGe detector. For any other closed-ended detector of a different dimension from this study, the present numerical analysis can be applied straightforwardly. The current approach, however, has a limiting assumption of single position for absorption of γ-ray energy. If the timing performance is measured by experimental arrangement of γ-ray detection, the interaction positions and absorbed energies are varied and dispersed in the detector [2,3,14]. Therefore a study of the signal risetime distribution in more realistic situation and a comparison with the actual measurement need further works and are planned for future.

The author is grateful to Dr. M.S. Kim for his proofreading of the draft of this paper.

References

1. K. Debertin and R.G. Helmer, *Gamma- and X-ray Spectrometry with Semiconductor Detectors*, p. 80, North-Holland, Amsterdam (1988)
2. J. Llacer, *Nucl. Instr. and Meth.* **98**, 259-268 (1972)
3. T.W. Raudorf, T.J. Paulus, M.O. Bedwell and M. Martini, *IEEE Trans. on Nucl. Sci.* **NS-24**, No. 1, 78-87 (1977)
4. T.W. Raudorf, M.O. Bedwell and T.J. Paulus, *IEEE Trans. on Nucl. Sci.* **NS-29**, No. 1, 764-768 (1982)
5. A. Alberigi Quaranta, M. Andretta and G. Zanarini, *IEEE Trans. on Nucl. Sci.* **NS-29**, No. 4, 1370-1376 (1982)
6. A. Alberigi Quaranta, A. Catellani, M. Cuzzilla and G. Zanarini, *IEEE Trans. on Nucl. Sci.* **NS-30**, No. 3, 1862-1869 (1983)
7. W.H. Press, B.P. Flannery, S.A. Teukolsky and W.T. Vetterling, *Numerical Recipes*, Chap. 17, Cambridge Univ. Press, Cambridge (1989)
8. J.S. Hornsby, *CERN Data Handling Division Report 63-7*, CERN, Geneva (1963)
9. B.A. Carré, *Computer Journal*, Vol. 4, No. 1 (1961)
10. Canberra Industries, Inc., *Germanium Detectors User's Manual* (1993)
11. G.F. Knoll, *Radiation Detection and Measurement*, 2nd Ed., p. 387, Wiley, Singapore (1989)
12. G. Ottaviani, C. Canali and A. Alberigi Quaranta, *IEEE Trans. on Nucl. Sci.* **NS-22**,

No. 1, 192-204 (1975)

13. H.I. Bak, Y.D. Bae, M.S. Kim and H.D. Choi, *Nucl. Instr. and Meth. in Phys. Res.* **A 366**, 332-339 (1995)
14. A. Alberigi Quaranta, A. Catellani, G. Pizziolo and G. Zanarini, *IEEE Trans. on Nucl. Sci.* **NS-31**, No. 1, 900-906 (1984)